Centrifuge investigation of pipeline uplift on sloping ground using a novel internal measurement technique

Z. Liu
Department of Engineering, University of Cambridge, Cambridge, UK, zl528@cam.ac.uk

S.K. Haigh
Department of Engineering, University of Cambridge, Cambridge, UK, skh20@cam.ac.uk

ABSTRACT: This study presents a series of centrifuge model tests conducted in the Mark-II mini-drum centrifuge to quantify the uplift resistance of buried pipelines under both horizontal and inclined ground conditions. Three tests were performed: two at varying embedment depths in level ground and one beneath a sloping surface. A newly developed internal measurement system was incorporated into the model pipe to directly capture uplift forces, enabling comparison with conventional external measurements. Results confirm that external measurements systematically overestimate uplift resistance, while the internal system provides a more representative assessment of soil–pipe interaction. Under inclined ground, the pipeline exhibited lower peak uplift resistance and noticeable lateral displacement. Particle Image Velocimetry (PIV) analyses indicate that reduced overburden stress, shorter shear-band development paths, and smaller vertical components of shear resistance contribute to the earlier onset of uplift on slopes compared with level ground. These findings highlight the importance of explicitly considering ground inclination and realistic measurement approaches in the design of buried pipelines crossing uneven terrain.

1 INTRODUCTION

With the continued expansion of petroleum extraction and long-distance energy transportation, upheaval buckling (UHB) remains a long-standing challenge for researchers and practitioners. Because pipelines are typically installed at near-ambient temperatures while transported hydrocarbons often reach elevated temperatures during operation, substantial thermal compressive stresses may develop. These stresses can induce vertical deformation and promote breakout of the pipeline from the confining soil cover. The limited soil mass directly above the pipeline commonly represents the weakest component of resistance, making accurate evaluation of uplift resistance essential for determining appropriate burial depth and soil conditions required for safe design.

Over the past decades, numerous analytical models have been developed to estimate uplift resistance. Matyas and Davis (1983) conceptualized the resistance as the weight of an inverted trapezoidal soil block above the pipe. Trautmann et al. (1985) included the contribution of shear forces acting on the uplifted soil mass. White et al. (2001) proposed that the resistance comprises both the weight of the inverted soil wedge and shear forces along the inclined shear band (Figure 1). More recently, Wu et al. (2021) demonstrated that uplift resistance becomes insensitive to increasing burial depth beyond a critical soil-cover-to-diameter ratio (H/D).

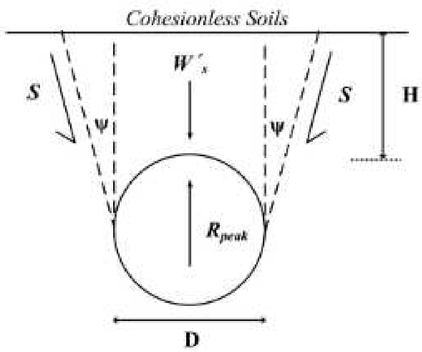

Figure 1. The inclined slip plane model. (White et al., 2001)

The initial uplift resistance can be decomposed into several components (Vesić, 1971):

1. the effective weight of the pipeline
2. the effective weight of the soil mass lifted above the pipeline
3. the vertical component of shear resistance along the shear band
4. cohesion between pipeline and soil and
5. suction effects associated with pore-pressure differences

Among these, the first three components are typically dominant. Cohesion is negligible for sandy soils, and suction effects can be disregarded for fully saturated sandy soils or cases involving long-term small displacements.

In addition to theoretical models, extensive physical and numerical investigations have been conducted, including full-scale 1g tests (Cheuk et al., 2008; Robert and Thusyanthan, 2018; Schaminee et al., 1990; Wu et al., 2021), centrifuge modelling (Dickin, 1994; Wang et al., 2011; White et al., 2001), and finite-element simulations (Bransby et al., 2001; Robert and Thusyanthan, 2018). However, existing work exhibits several limitations:

1. uplift resistance is commonly measured externally using load cells, which tend to overestimate pipe resistance.
2. the 3D pipe section tests introduce additional frictional forces at both pipe ends.
3. Many experiments assume a level ground surface, offering limited insight into pipelines traversing sloping or undulating terrain.

To address these gaps, the present study idealizes the UHB problem as a plane-strain condition and introduces a novel internal measurement technique to directly capture uplift forces. A series of centrifuge model tests were then conducted to investigate pipeline uplift behaviour beneath sloping ground, with the aim of providing more realistic insight into soil–pipeline interaction under non-level surface conditions.

2 METHODOLOGY

This study employed the Mark II mini-drum centrifuge to investigate the uplift behaviour of a buried pipeline under both level and sloping ground conditions. Uplift was induced by a uniaxial actuator that displaced the pipeline vertically at a constant rate. A newly developed internal measurement system was integrated within the model pipe to directly quantify soil resistance, supplemented by displacement measurements using a Linear Variable Differential Transformer (LVDT) and particle-scale deformation tracking using a Raspberry Pi camera and GeoPIV-RG.

2.1 Mark II mini-drum centrifuge

The Mark II mini-drum centrifuge at the Schofield Centre, University of Cambridge (Figure 2 and 3), is designed for small-scale geotechnical modelling. The device consists of a ring channel with a base radius of 370 mm and can generate up to 471 g at 1067 rpm. The system includes a 16-channel data acquisition unit (sampling up to 10 kHz), in-flight video recording capabilities, and actuators capable of radial or circumferential loading.

A central pivot enables rotation of the channel axis by 90°, allowing horizontal model preparation and vertical testing. Water supply and drainage are controlled via an adjustable standpipe. Detailed specifications are provided in Barker (1998). The model container is partitioned into a model chamber and a sensor chamber, separated by a transparent glass window. The chamber depth is 150 mm with a central angle of 52°.

Figure 2. The Mini-drum Centrifuge setup.

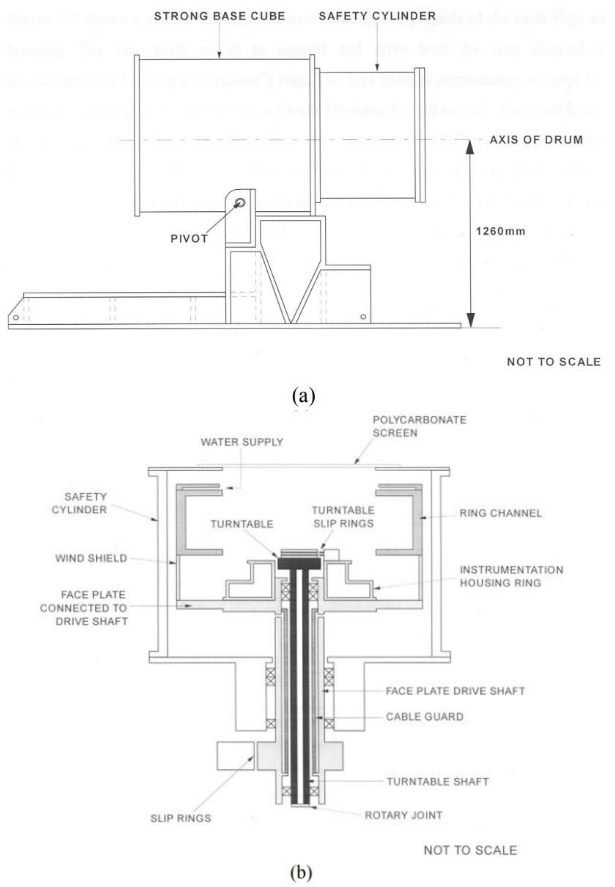

Figure 3. The Mini-drum Centrifuge (a)elevation and (b) cross-section. (Wang et al., 2009)

2.2 Internal pipeline measurement system

A four-component pipeline assembly (Figure 4) was developed to enable direct measurement of uplift resistance within the pipe. The assembly consists of:

1. Flexible steel cable – connecting the actuator to the frame and accommodating minor rotational freedom during uplift.
2. Aluminium balancing bar – dividing the actuator's single-point load equally into two symmetric forces to ensure translational pipeline motion.
3. Copper connecting rods – smooth, low-friction shafts transmitting load to the internal beam while minimizing soil–rod interaction.
4. Pipeline body – composed of an aluminium casing, internal load-bearing beam, and end caps joining the casing and beam.

A critical design feature is that the connecting rods are attached exclusively to the internal load-bearing beam and have no contact with the pipe casing. Thus, all forces transmitted into the load-bearing beam originate solely from soil–pipe interaction.

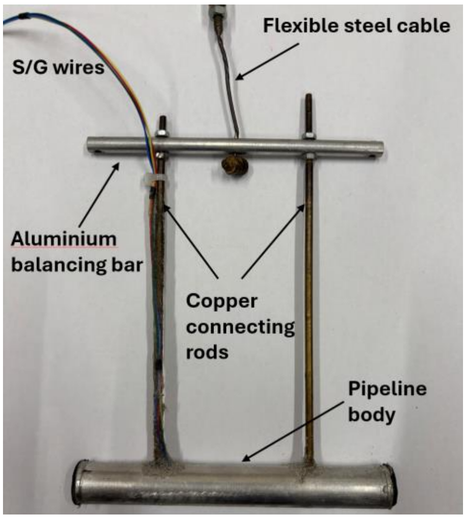

(a)

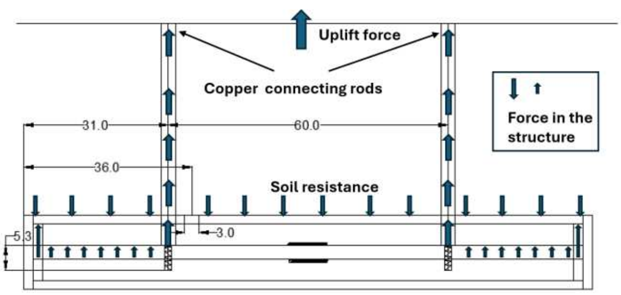

(b)

Figure 4. (a) The setup of the internal measurement pipe (b) the schematic cross-section of the pipe.

2.2.1 Measurement principle

The soil resistance is inferred from the bending strain at the mid-span of the internal load-bearing beam, measured using a full-bridge strain gauge circuit (Figure 5). The bending strain ε relates to the bending moment M by:

$$\varepsilon = \frac{\sigma}{E} = \frac{My}{EI} = \frac{M \times \frac{d}{2}}{E \times \frac{bd^3}{12}} = \frac{6M}{Ebd^2} \tag{1}$$

and the bending moment is

$$M = l \times S \tag{2}$$

where $E(Pa)$ is elastic modulus, $M(N \cdot m)$ is the bending moment, $y(m)$ is the perpendicular distance from the neutral axis, $I(m^4)$ is the second moment of area, $b(m)$ and $d(m)$ are beam dimensions, $l(m)$ is the lever arm, and $S(N)$ is the shear force transmitted through the connecting rods.

Because the shear force transmitted from the rods to the load-bearing beam equals the soil-induced resistance, the mid-span strain provides a direct measure of uplift resistance. Calibration of strain gauge voltage against known external loads enables conversion to soil resistance during testing.

(a)

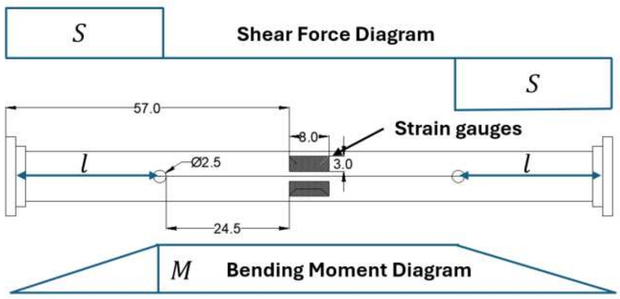

(b)

Figure 5. (a) The setup of load-bearing beam inside the pipe (b) the schematic setup of load-bearing beam.

2.3 Actuator system

Uplift displacement was imposed using a 24 V DC motor driving a lead screw through a gearbox, enabling controlled vertical movement of the loading frame (Figure 6). The system provides travel speeds from 0.002 mm/s to 0.2 mm/s and a total stroke of 120 mm. An LVDT fixed to the actuator recorded displacement of loading plate. A load cell fixed to the loading plate recorded force applied by actuator.

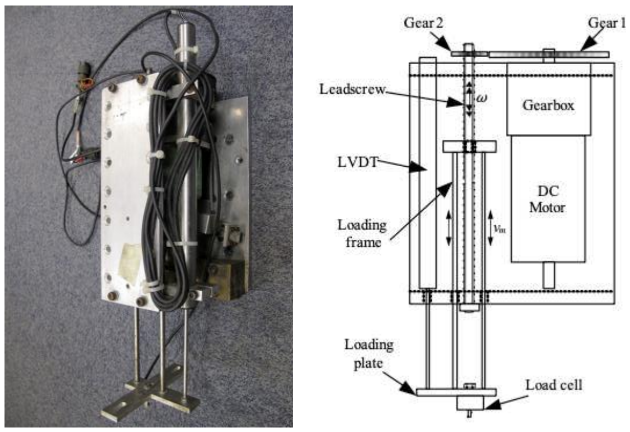

(a) (b)

Figure 6. (a) The setup of the actuator and the LVDT (b) the schematic setup of the actuator and the LVDT. (Wang et al., 2012)

2.4 Raspberry-pi camera and GeoPIV-RG

A Raspberry Pi microcomputer equipped with a high-resolution camera captured images of the soil through the glass window on the sensor side of the container at 5-second intervals. Communication with the Raspberry Pi was maintained through the mini-drum's slip-ring via Ethernet, permitting remote control using SSH and real-time image transfer via shared folders.

The PIV tool used in this study was GeoPIV-RG, created by Stanier et al. (2016). It enables the creation of a photo mesh, capturing the coordinates of each mesh point. By comparing data from different photographs, it determines the displacement of soil particles.

2.5 Material

The model pipeline was fabricated from aluminium alloy 6082. The soil used in all experiments was HN31 Hostun sand, prepared at approximately 3% water content and loose to medium relative density. Key material properties are summarised in Table 1.

Table 1. Properties of Hostun sands. (Chian et al., 2010)

ϕ_{crit}	D_{10}	D_{50}	D_{60}	e_{min}	e_{max}	G_s
33°	0.209 mm	0.335 mm	0.365 mm	0.555	1.01	2.65

2.6 Model set-up

The pipeline was embedded perpendicular to both the model container wall and the glass observation panel, with the upper end connected to the load cell on the actuator positioned at the centrifuge centre (Figure 7). Ground surfaces were prepared either horizontal or inclined, depending on the test condition.

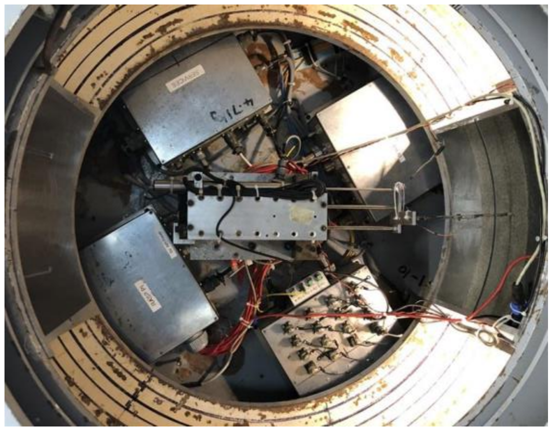

(a)

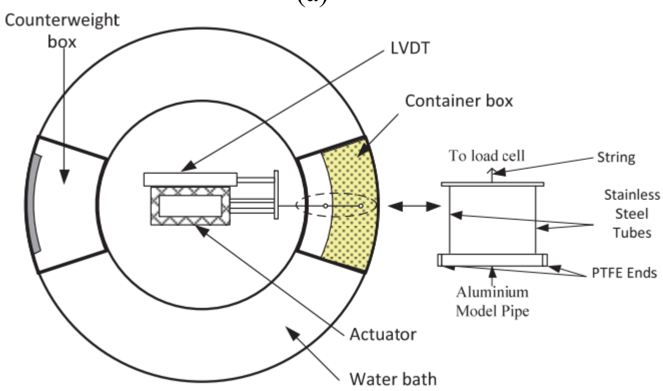

(b)

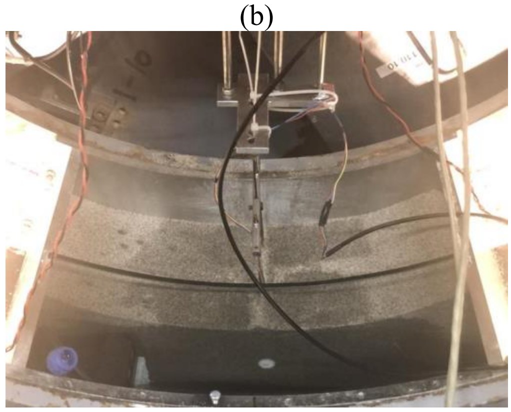

(c)

Figure 7. (a) The setup of the mini-drum interior (b)the schematic setup of the mini-drum interior (Wang et al., 2011), and (c)the setup of UHB model.

2.7 Model preparation and test procedure

2.7.1 Model preparation

1. Spread Hostun sand to the elevation of the pipe.
2. Install the pipe at the target embedment depth.
3. Spread additional sand to the intended ground level.
4. Saturate the model from the container base.
5. Form the ground surface: either shaped curved surface or constructed as a stepped slope matching calculated geometry.
6. Install counterweights according to model mass requirements.
7. Mount the container on the centrifuge.
8. Configure DASYLab data acquisition and Raspberry Pi imaging.

2.7.2 Test procedure

1. Rotate the mini-drum 90° from the preparation position to the vertical testing position.
2. Ramp up to 10 g to confirm stability of all sensors and connections.
3. Increase to the target acceleration level.
4. Initiate pipeline uplift via the actuator at 0.037 mm/s.
5. Stop actuator once the pipe reaches ground level and decelerate the centrifuge to rest.

2.8 Testing Programme

Three centrifuge model tests were conducted using Hostun sand at loose to medium relative density. Two tests were run under level-ground conditions with H/D ratios of 2 and 1, respective and one test under a 20° inclined surface with H/D = 1. Test programme details are shown in Table 2.

Table 2. Experimental parameters and soil conditions for Tests 1–3.

	Test1	Test2	Test3
g-level	20.8	20.8	20.8
H/D	2	1	1
Slope°	0	0	20
$\boldsymbol{w}$(%)	3.23	2.87	3.36
Dr(%)	34.66	47.27	49.84

3 TEST RESULTS AND DISCUSSION

3.1 Soil uplift resistance

Four normalised uplift force-displacement curves were obtained in this study (Figure 8). Soil resistance was normalised by dividing the measured force F by effective soil unit weight γ', burial depth H, pipe diameter D, and pipe length L, while displacement Y was normalised by pipe diameter. Because the pipe was ultimately dragged to the ground surface, the displacement endpoints in all curves converge. The figure presents the external and internal measurements from Test 1, as well as the internal measurements from Tests 2 and 3.

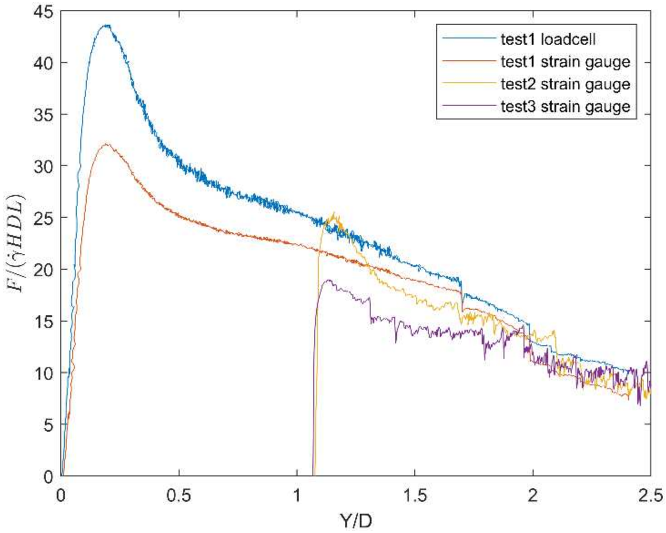

Figure 8. Normalized uplift force-displacement response from test1-3.

The uplift force-displacement curves show that uplift behaviour generally progresses through three distinct phases. In Phase I, small vertical displacement leads to a rapid increase in resistance until the peak is reached. Phase II begins immediately after peak mobilisation, during which resistance decreases sharply. Phase III is characterised by a more gradual reduction in resistance prior to surface breakthrough.

The two curves from Test 1 show that the externally measured peak resistance exceeds the internal measurement by 37.5%. This difference arises because external measurements include soil resistance together with the pipe's self-weight, the towing frame weight, frame–soil friction, and sidewall friction. Internal measurements exclude frame–soil friction. As the pipe approaches the surface, the frame–soil friction decreases approximately linearly with burial depth, which explains the convergence of the external and internal curves at ground level.

The data from Test 2 show that its peak resistance is larger than the resistance recorded for Test 1 at the same burial depth. However, the resistance values from the two tests gradually converge during Phase III.

In comparison, the peak resistance of Test 3 is 33.5% lower than that of Test 2. In addition, the gradient of reduction of test 3 in the post-peak stage is smaller, the transition to Phase III is less distinct, and the curve exhibits more noise.

(a) (b)

Figure 9. (a) Overview of model after test 3 (b) the deposit formed on the pipe.

For soils of low water content, triangular soil wedges commonly form on the pipe surface after breakthrough. In Test 3, soil deposits reached a height of 1.26D above the pipe after uplift (Figure 9).

In centrifuge testing, the final uplift resistance should theoretically be lower than the self-weight of the pipe at the model g-level, because upward pipe movement reduces the centrifugal force acting on it. However, soil deposition above the pipe and sidewall friction maintained a final resistance larger than the pipe weight.

3.2 Soil-pipe interaction mechanism

A total of seven datasets were analysed. Each dataset includes soil particle displacement vector fields for visualising particle trajectories, and displacement contour plots for identifying shear band development. Test 1 comprises three datasets: 0–1.7 mm (pre-peak), 1.7–2.6 mm (post-peak), and 15.8–16.7 mm (H/D = 1 condition) (Figure 10). Test 2 includes two datasets: 0–0.9 mm (pre-peak) and 0.9–1.7 mm (post-peak) (Figure 11). Test 3 also includes two datasets: 0–1.3 mm (pre-peak) and 1.3–2.8 mm (post-peak) (Figure 12).

Additionally, both image dimension, plot dimensions and displacement measurements have been calibrated from pixels to actual millimetre units. A 1 mm scale vector bar is also provided in the upper right corner of each vector plot.

3.2.1 Test 1

During the pre-peak stage (Figure 10 (a) & (b)), the vector fields show that the affected soil mass forms an inverted trapezoidal zone extending from the pipe crown to the ground surface. Soil particles above the pipe move vertically upwards, with vector directions rotating laterally and displacement magnitudes diminishing with horizontal distance from the pipe. The contour plots show convex, upward-facing displacement isosurfaces, indicating that the region directly above the pipe undergoes compression before significant displacement occurs elsewhere

During the post-peak stage (Figure 10 (c) & (d)), soil displacement becomes more uniform, and a shear zone develops at an angle of 5–14° from the vertical. The reduction in soil resistance during this stage is therefore attributed to shear band development, which disrupts interparticle interlocking and reduces shear capacity.

At H/D = 1 (Figure 10 (e) & (f)), the low water content (~3%) generates notable suction forces. The void created beneath the rising pipe does not collapse, a surface mound develops, and a prominent shear band forms. The deformation zone is concentrated directly above the pipe.

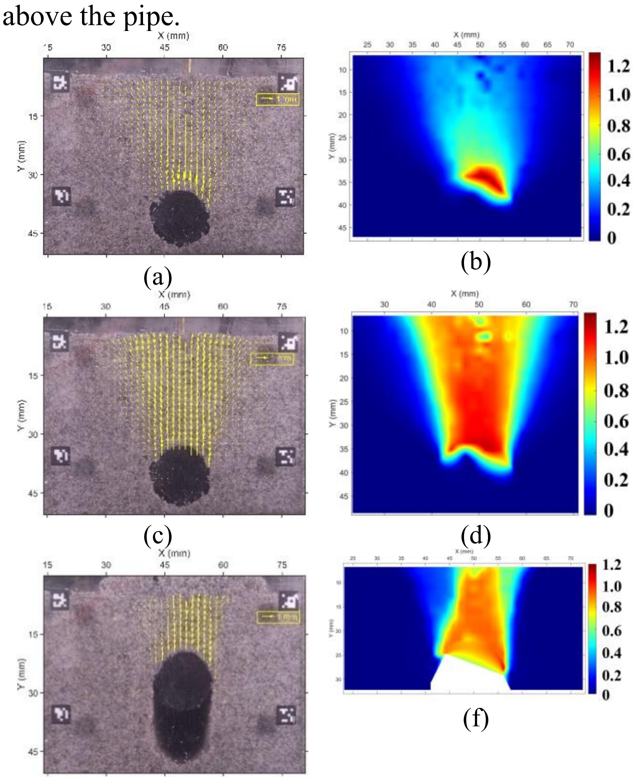

(a) (b) (c) (d) (e) (f)

Figure 10. The soil particle displacements vector and contour plots from test 1 at (a)(b)pre-peak stage, (c)(d)post-peak stage, and (e)(f)after H/D<1.

3.2.2 Test 2

The pre-peak (Figure 11(a) & (c)) and post-peak (Figure 11 (b) & (d)) responses of Test 2 exhibit similar features to Test 1 namely, soil compression followed by shear band formation. However, the deformation zone is more localised above the pipe, and the shear band develops almost vertically. This behaviour is attributed to the shallower burial depth, which limits the development of a broader compression zone. The higher peak resistance in Test 2 compared with Test 1 arises because the shear band had not yet formed during the pre-peak phase.

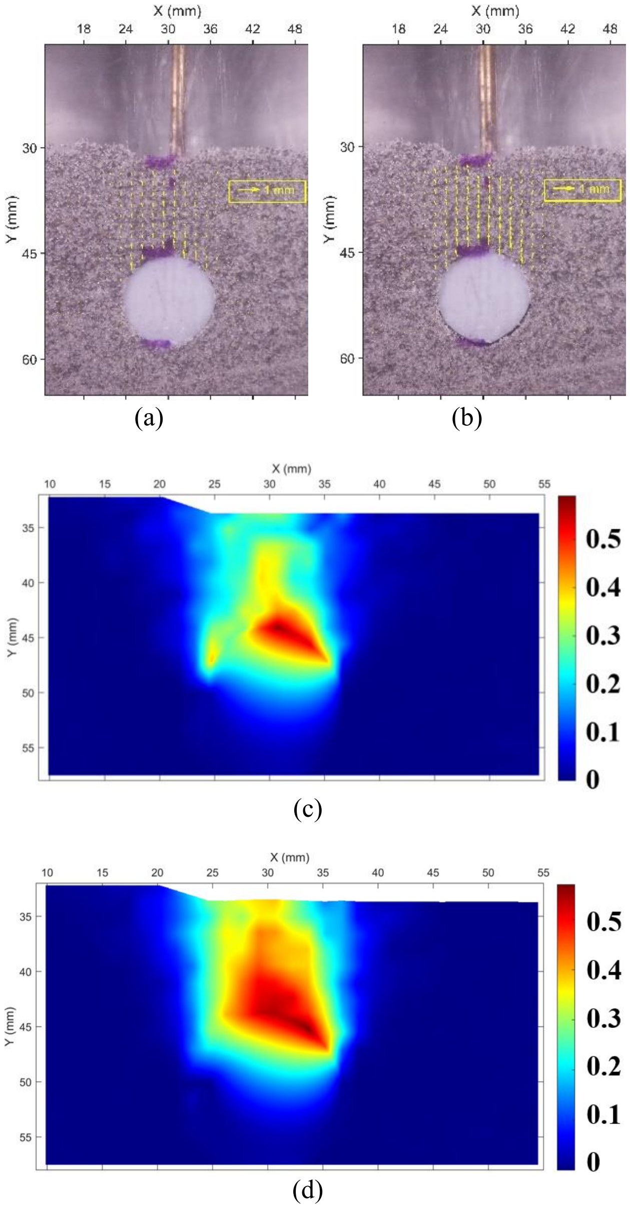

Figure 11. The soil particle displacements vector and contour plots from test 2 at (a)(c)pre-peak stage (b)(d)post-peak stage.

3.2.3 Test 3

In Test 3, both pre-peak compression (Figure 12(a) & (c)) and post-peak shear banding (Figure 12(b) & (d)) are observed. The key difference is that, for the same pipe displacement, soil movements are smaller in the pre-peak stage than that in post-peak stage. Soil particles tend to move in the direction perpendicular to the ground slope rather than vertically upward, resulting in shorter shear bands that are oriented normal to the slope surface. The post-peak image reveals lateral displacement of the pipe to the left, despite the actuator applying a vertical force.

These findings indicate that the reduced uplift resistance under sloping ground arises from the shorter path length required for the pipe to reach the surface. Simultaneously, unbalanced lateral earth pressures induce lateral pipe displacement.

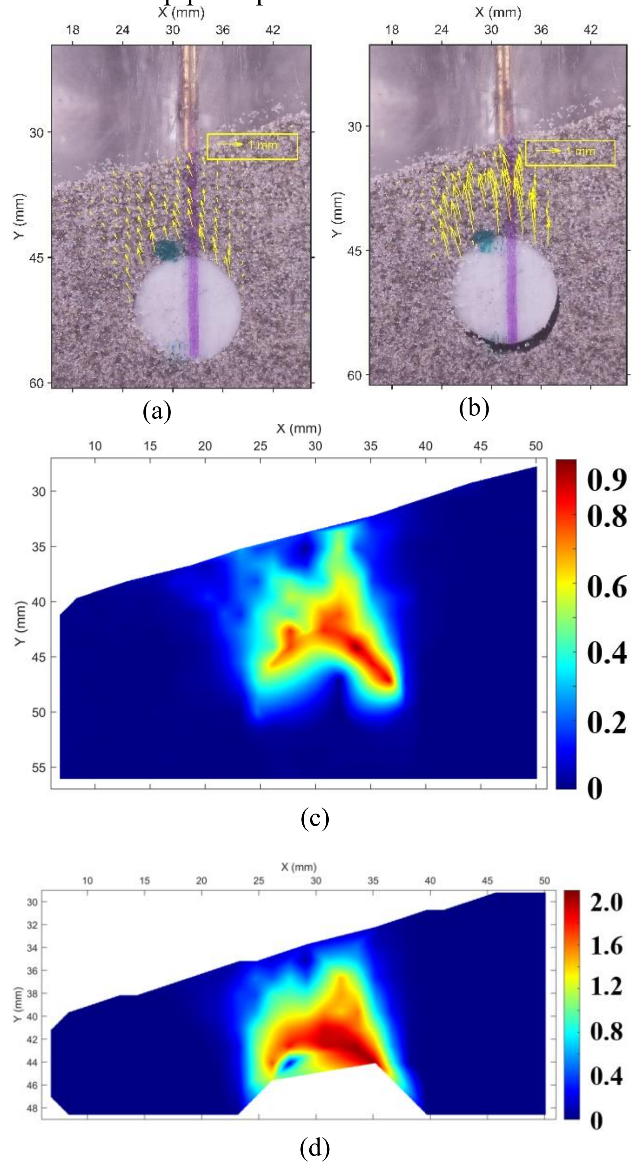

Figure 12. The soil particle displacements vector and contour plots from test 3 at (a)(c)pre-peak stage (b)(d)post-peak stage.

3.3 Pipe mobilised displacements

Table 3 summarises the pipe displacements required to reach peak soil resistance, based on combined PIV and LVDT analysis. Pipelines buried at greater depths require larger uplift displacements to mobilise peak resistance, whereas pipelines beneath slopes also exhibit increased displacement demand. All values of y_{peak} fall within the range 0.05D–0.11D.

Table 3. Peak displacement during uplift.

	Test1	**Test2**	**Test3**
$y_{peak}(mm)$	1.7	0.9	1.3
y_{peak}/D	0.11	0.057	0.085

4 CONCLUSIONS

Based on three centrifuge experiments investigating UHB behaviour under different burial depths and slope conditions, the following conclusions are drawn:

1. External uplift measurements significantly overestimate true soil resistance. They incorporate frame–soil friction, leading to substantial overestimation. Innovative experimental design is essential, and internal pipe measurement methods can be applied to a broader range of experiments.
2. Deeper burial conditions cannot be used to infer shallow-burial uplift mechanisms. The underlying soil displacement patterns differ fundamentally: deeper burial promotes broader compression zones and inclined shear bands, whereas shallow burial leads to vertically oriented shear failure.
3. Pipelines beneath sloping ground exhibit higher uplift vulnerability. Slopes reduce soil resistance, increase the displacement required to reach peak resistance, and trigger lateral pipe movement due to asymmetric earth pressures. Vertical and lateral resistance components can be calculated from observed lateral displacement.
4. The formation of shear bands marks the primary distinction between pre-peak and post-peak. Soil resistance decreases significantly once shear bands develop, indicating a transition from compressive to shear-dominated behaviour.
5. Pipes at greater burial depths or beneath slopes require larger displacements to mobilise peak soil resistance. Across all tests, peak normalised displacements fall within the range 0.05D–0.11D.

REFERENCES

Barker, H. R. (1998). *Physical modelling of construction processes in the mini-drum centrifuge* (Doctoral dissertation, University of Cambridge).

Bransby, M. F., T. A. Newson, P. Brunning, and M. C. R. Davies (2001). Numerical and centrifuge modelling of the upheaval resistance of buried pipelines. *In Proceedings of OMAE pipeline symposium, Rio de Janeiro.*

Cheuk, C. Y., D. J. White, and Malcolm D. Bolton (2008). Uplift mechanisms of pipes buried in sand. *Journal of geotechnical and geoenvironmental engineering* 134.2: 154-163. https://doi.org/10.1061/(ASCE)1090-0241(2008)134:2(154)

Chian, S. C., M. E. Stringer, and S. P. G. Madabhushi (2010). Use of automatic sand pourers for loose sand models. Proceedings of the 7th International Conference on Physical Modelling in Geotechnics, 7th ICPMG'10, pp. 117-121. Zurich, Switzerland.

Dickin, E. A. (1994). Uplift resistance of buried pipelines in sand. *Soils and foundations*, 34(2), 41-48. https://doi.org/10.3208/sandf1972.34.2_41

Matyas, E. L., and J. B., Davis (1983). Prediction of vertical earth loads on rigid pipes. *Journal of Geotechnical Engineering*, 109(2), 190-201. https://doi.org/10.1061/(ASCE)0733-9410(1983)109:2(190)

Robert, D. J., and N. I. Thusyanthan (2018): Uplift resistance of buried pipelines in partially saturated sands. *Computers and Geotechnics* 97 7-19. https://doi.org/10.1016/j.compgeo.2017.12.010

Stanier, S., J. Dijkstra, D. Leśniewska, J. Hambleton, D. White, and D. M. Wood (2016). Vermiculate artefacts in image analysis of granular materials. *Computers and Geotechnics*, 72, 100-113. https://doi.org/10.1016/j.compgeo.2015.11.013

Schaminee, P. E. L., N. F. Zorn, and G. J. M. Schotman (1990). Soil response for pipeline upheaval buckling analyses: full-scale laboratory tests and modelling. *Offshore Technology Conference*. OTC, 1990. https://doi.org/10.4043/6486-MS

Trautmann, C. H., T. D. O'Rourfce, and F. H. Kulhawy, (1985). Uplift force-displacement response of buried pipe. *Journal of Geotechnical Engineering*, 111(9), 1061-1076. https://doi.org/10.1061/(ASCE)0733-9410(1985)111:9(1061)

Vesić, A. S. (1971). Breakout resistance of objects embedded in ocean bottom. *Journal of the Soil Mechanics and Foundations Division*, 97(9), 1183-1205. https://doi.org/10.1061/JSFEAQ.0001659

Wang, J., S. K. Haigh, G. Forrest, and N. I. Thusyanthan (2012). Mobilization distance for upheaval buckling of shallowly buried pipelines. *Journal of Pipeline Systems Engineering and Practice*, 3(4), 106-114. https://doi.org/10.1061/(ASCE)PS.1949-1204.0000099

Wang, J., S. K. Haigh, and N. I. Thusyanthan (2011). Pipeline Uplift Response in Thawed Sandy Backfills: Preliminary Findings. *ISOPE International Ocean and Polar Engineering Conference. ISOPE.*

Wang, J. (2012). *Monotonic and cyclic uplift resistance of buried pipelines in cohesionless soils* (Doctoral dissertation, University of Cambridge).

Wang, J., S. K. Haigh, and N. I. Thusyanthan (2009). Uplift resistance of buried pipelines in blocky clay backfill. *ISOPE International Ocean and Polar Engineering Conference. ISOPE.* https://doi.org/10.4043/20912-MS

White, D. J., A. J. Barefoot, and M. Bolton (2001). Centrifuge modelling of upheaval buckling in sand. *International Journal of Physical Modelling in Geotechnics* 1.2: 19-28. https://doi.org/10.1680/ijpmg.2001.01020

Wu, J., G. Kouretzis, and L. Suwal(2021). Bearing capacity mechanisms for pipes buried in sand. *Canadian Geotechnical Journal,* 58(6), 834-847. https://doi.org/10.1139/cgj-2020-0109